Journal of Asian Earth Sciences 39 (2010) 335–346

Contents lists available at ScienceDirect

Journal of Asian Earth Sciences

journal homepage: www.elsevier.com/locate/jseaes

U–Pb and Hf isotope analyses of detrital zircons from Late Paleozoic sediments: Insights into interactions of the North China Craton with surrounding plates

Hong-Yan Li [a,b,*], Bin He [a], Yi-Gang Xu [a], Xiao-Long Huang [a]

[a] Key Laboratory of Isotope Geochronology and Geochemistry, Guangzhou Institute of Geochemistry, Chinese Academy of Sciences, Guangzhou 510640, China
[b] Laboratory for Metallogenic Dynamics, Guangzhou Institute of Geochemistry, Chinese Academy of Sciences, Guangzhou 510640, China

ARTICLE INFO

Article history:
Received 24 December 2009
Received in revised form 23 April 2010
Accepted 14 May 2010

Keywords:
Detrital zircon
U–Pb and Hf isotopes
Provenance analysis
North China Craton

ABSTRACT

U–Pb dating and Hf isotope analyses were performed on detrital zircons from the Upper Permian sandstones in the Ordos and Jiyuan basins, with aims of defining the sediment provenance, and by inference, to determine the influence of the surrounding plates on the evolution of the North China Craton (NCC). Detrital Zircons from these two basins fall into three major groups based on their U–Pb ages: Phanerozoic, Paleoproterozoic, and Neoarchean. The youngest grain from every sample is only slightly younger than the real depositional age of strata. The Phanerozoic zircons from the Jiyuan basin (244–390 Ma) show $\varepsilon_{Hf}(t)$ ranging from −30.3 to −1.3, suggesting a provenance from the Inner Mongolia Paleo-uplift (245–376 Ma, $\varepsilon_{Hf}(t) = -18.9$ to −1.7). A bi-modal distribution of ages and $\varepsilon_{Hf}(t)$ is noted for detrital zircons from the Ordos basin; one resembles that of the Jiyuan basin, the other is characterized by Early Paleozoic ages and relatively high $\varepsilon_{Hf}(t)$ values (−10.9 to 7.7). A hybrid source is thus inferred for the Ordos sediments; the Northern Qinling Orogen (428–478 Ma, $\varepsilon_{Hf}(t) = -10.9$–7.7) must have served as a source in addition to the Inner Mongolia Paleo-uplift source. This interpretation is consistent with the fact that the Northern Qinling Orogen was an active margin during the Early Paleozoic and suggests that the western part of the Northern Qinling Orogen was elevated relative to the center of the craton during the Late Paleozoic. It is likely that the Early Paleozoic arc-trench in the northern part of the Dabie Orogen was under-thrusted below the NCC due to the subduction of the Yangtze plate during the Triassic. The Inner Mongolia Paleo-uplift was strongly uplifted by subduction of the Paleo-Asian Ocean Plate underneath the northern NCC and functioned as a sediment source for the inner craton during the Late Paleozoic. These results reveal a heterogeneous pattern of destruction of the North China Craton, with its northern margin starting to be activated no later than Late Paleozoic.

1. Introduction

Integration of geology, geophysics and geochemistry has provided clues to understanding the evolution of North China Craton (NCC) (e.g., Menzies et al., 2007). It has been argued that the NCC has lost >120 km thick lithosphere during the Late Mesozoic (Fan and Menzies, 1992; Griffin et al., 1992; Menzies et al., 1993; Gao et al., 2004; Xu, 2001; Xu et al., 2004a,b). This cratonic destruction was associated with widespread magmatism, intraplate deformation, and large scale mineralization (Mao et al., 2003; Zhang et al., 2003; Xu et al., 2009). Among the remaining questions are the actual timing of the destruction of the NCC and the influence of surrounding plate movement on the evolution of the NCC (Wu et al., 2008; and references therein).

Provenance analysis of sedimentary rocks can provide important constraints on the dynamics of basin formation and orogenic processes. In particular, it can yield information that clarifies the large-scale movement of crustal blocks (Li et al., 2004, 2005, 2009; Yang et al., 2006). Reading the sedimentary record provides clues that help to understand deep earth processes. Good examples for this approach include the Emeishan large igneous province, where plume-induced pre-volcanic crustal doming is registered in underlying limestones and surrounding clastic sedimentary deposits (He et al., 2003, 2007). Another example is the uplift of the Yanshan Orogenic Belt, which coincided with a significant shift of the sedimentary provenance of the Xishan basin during Late Mesozoic (Yang et al., 2006). The dramatic change in lithospheric architecture beneath the NCC is thus expected to be recorded in surface geological processes. With this purpose in mind, we have

* Corresponding author at: Key Laboratory of Isotope Geochronology and Geochemistry, Guangzhou Institute of Geochemistry, Chinese Academy of Sciences, Guangzhou 510640, China. Tel.: +86 20 85290401; fax: +86 20 85290261.
E-mail address: hongyanli@gig.ac.cn (H.-Y. Li).

1367-9120/$ - see front matter © 2010 Elsevier Ltd. All rights reserved.
doi:10.1016/j.jseaes.2010.05.002

performed provenance analysis of the latest Paleozoic Formations, the Permian sandstones of the Ordos and Jiyuan basins.

Zircon possesses the highest closure temperature of the U–Pb and Lu–Hf isotopic systems among all known minerals (about 900 °C) (Kinny and Maas, 2003; Wu and Zheng, 2004) and is relatively immune to subsequent surface geological events (Wu et al., 2007). Consequently, combined U–Pb age spectrum and Hf isotopic data of detrital zircons can yield reliable information about sediment provenance and enable paleogeographic reconstruction (Bruguier et al., 1997; Bodet and Scharer, 2000; Richards et al., 2005). This paper reports *in situ* LA-ICP-MS U–Pb and Neptune MC-ICPMS Hf isotope analyses on zircons of Upper Permian sandstone from the Ordos and Jiyuan basins. The data will be used to discuss the effects of the kinematics of surrounding plates on the evolution of the NCC.

2. Geological setting and sampling

The NCC, located south of the Xing-Meng Orogenic Belt (eastern part of the Central Asian Orogenic Belt), borders the Pacific in the east, connects with the Tarim craton in the west, and is separated from the Yangtze plate by the Qinling-Dabie Orogen. The latter is divided into the Northern and Southern Qinling Orogens, separated from one another by the Shangdan suture zone (Che et al., 2002). The Northern and Southern Qinling Orogen are regarded as the southern margin of the NCC and northern margin of the Yangtze plate, respectively (Fig. 1).

The northern margin of the NCC is marked by the Inner Mongolia Paleo-uplift to the north and the Yinshan-Yanshan belt to the south, separated by the Pingquan – Gubeikou – Chicheng – Shangyi fault (Fig. 1) (Che et al., 2002). To the north of the Inner Mongolia Paleo-uplift runs the Central Asian Orogenic Belt. The coupling between mountain building of the Central Asian Orogenic Belt and plate interaction between the NCC and the Paleo-Asian Ocean is complicated and controversial. Recent research has revealed that the Inner Mongolia Paleo-uplift was an active continental margin during the Late Paleozoic with subduction of the Paleo-Asian Ocean, which ended with ocean closed during the Late Permian – Early Triassic (Davis et al., 2001; Xiao et al., 2003; Zhang et al., 2007a).

Silurian, Devonian and part of the Early Carboniferous are absent from NCC sediments because of the uplift of the NCC during the Late Early Paleozoic, the oldest, pre-orogeny strata being Cambrian and Early to Middle Ordovician epicontinental carbonate sediments. The NCC subsided again after the Early Paleozoic, as indicated by transgressional deposits of clastic and marine sediments that become coal bearing during the Late Carboniferous and eventually continental during the Permian. The Late Paleozoic strata are the Benxi and Taiyuan Formations of the Late Carboniferous, the Shanxi and Xiashihezi Formations of the Early Permian, and the Shangshihezi and Shiqianfeng Formations of the Late Permian (Che et al., 2002).

We selected two sampling localities in view of their relatively complete preservation and the good exposure of Late Paleozoic

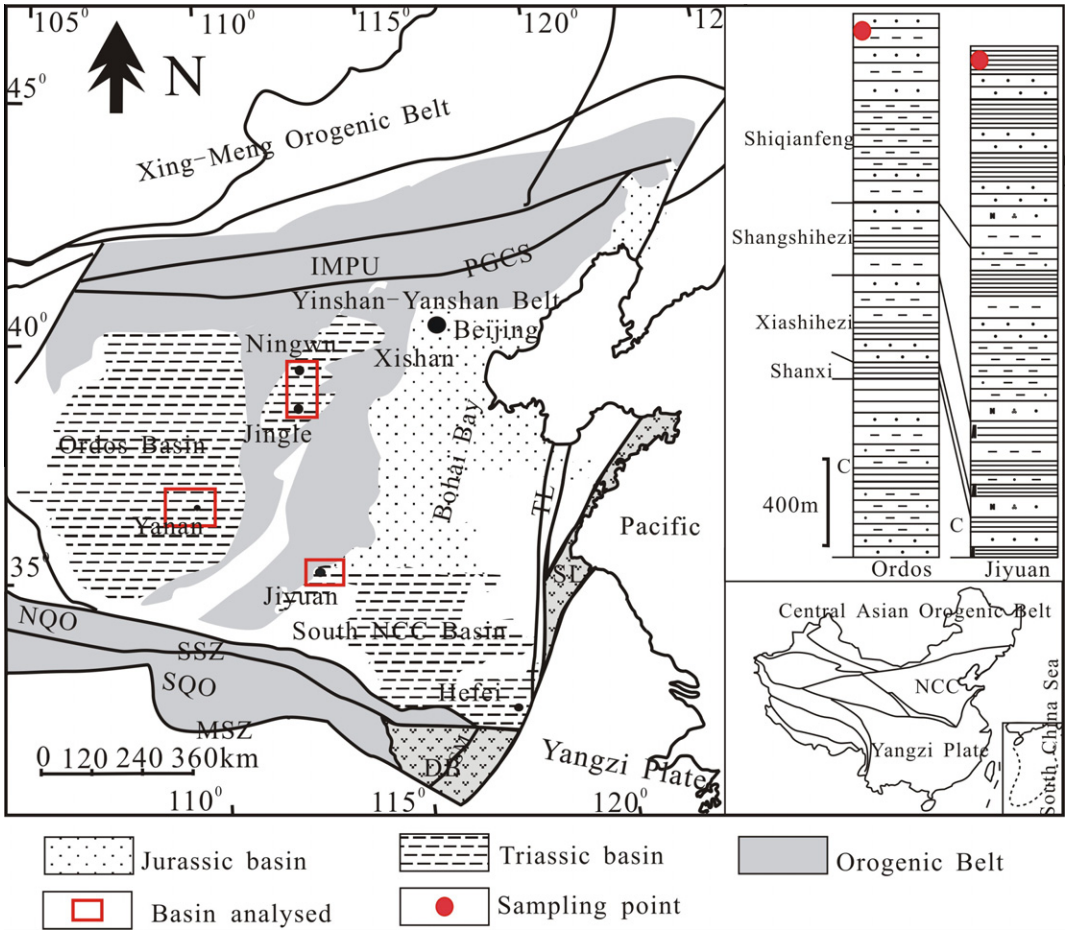

Fig. 1. Simplified tectonic map of the North China Craton and sampling licalities NCC: North China Craton NQO: Northern Qinling Orogen SQO: Southern Qinling Orogen SSZ: Shangdan suture zone MSZ: Mianlue suture zone DB: Dabie Orogen SL: Sulu Orogen IMPU: Inner Mongolia Paleo-uplift PGCS: Pingquan-Gubeikou-Chicheng-Shangyi Fault TL: Tanlu fault zone.

Table 1
LA-ICP-MS U–Pb dating results of detrital zircons.

Spots	Element (ppm)		Th/U	Isotopic ratios						Apparent age (Ma)					
	U	Th		$^{207}Pb/^{206}Pb$	1σ	$^{207}Pb/^{235}U$	1σ	$^{206}Pb/^{238}U$	1σ	$^{207}Pb/^{206}Pb$	1σ	$^{207}Pb/^{235}U$	1σ	$^{206}Pb/^{238}U$	1σ
J-5–01	1191	640	0.54	0.1726	0.0018	5.703	0.071	0.2397	0.0030	2583	9	1932	11	1385	15
J-5–02	519	542	1.05	0.1789	0.0019	7.053	0.090	0.2859	0.0035	2643	10	2118	11	1621	18
J-5–04	59	54	0.92	0.1653	0.0018	10.77	0.14	0.4723	0.0059	2511	10	2503	12	2494	26
J-5–05	37	25	0.67	0.1576	0.0019	9.389	0.127	0.4321	0.0054	2430	10	2377	12	2315	24
J-5–06	88	39	0.45	0.1664	0.0018	11.43	0.15	0.4982	0.0062	2522	10	2559	12	2606	27
J-5–07	57	62	1.08	0.1658	0.0019	10.60	0.14	0.4638	0.0058	2516	10	2489	12	2456	25
J-5–08	22	16	0.73	0.1290	0.0022	6.258	0.113	0.3519	0.0047	2084	15	2013	16	1944	23
J-5–09	17	25	1.43	0.1636	0.0022	10.26	0.15	0.4549	0.0059	2493	11	2458	14	2417	26
J-5–10	128	99	0.77	0.1622	0.0017	10.45	0.13	0.4672	0.0058	2479	10	2475	12	2471	25
J-5–11	70	112	1.60	0.1652	0.0018	10.55	0.14	0.4629	0.0058	2510	10	2484	12	2452	25
J-5–12	139	87	0.63	0.05579	0.00227	0.3353	0.0128	0.04359	0.00060	444	93	294	10	275	4
J-5–13	91	127	1.39	0.1716	0.0020	12.48	0.17	0.5274	0.0066	2573	10	2641	13	2730	28
J-5–14	334	139	0.42	0.1628	0.0017	10.23	0.13	0.4557	0.0056	2485	10	2455	12	2421	25
J-5–15	486	198	0.41	0.1588	0.0017	9.914	0.125	0.4529	0.0056	2443	10	2427	12	2408	25
J-5–16	61	42	0.69	0.1733	0.0019	11.55	0.15	0.4835	0.0060	2590	10	2569	12	2542	26
J-5–17	158	45	0.28	0.1641	0.0018	10.63	0.14	0.4698	0.0058	2499	10	2491	12	2483	26
J-5–18	95	62	0.65	0.1071	0.0012	4.458	0.060	0.3020	0.0038	1750	11	1723	11	1701	19
J-5–19	845	1275	1.51	0.1625	0.0017	9.724	0.122	0.4340	0.0054	2482	10	2409	12	2324	24
J-5–20	227	74	0.33	0.1635	0.0017	10.44	0.13	0.4631	0.0058	2492	10	2474	12	2453	25
J-5–21	798	306	0.38	0.1650	0.0017	11.23	0.14	0.4938	0.0061	2507	10	2543	12	2587	26
J-5–22	113	396	3.50	0.1662	0.0018	11.05	0.14	0.4822	0.0060	2519	10	2527	12	2537	26
J-5–23	178	85	0.48	0.05358	0.00092	0.3021	0.0052	0.0409	0.0005	353	20	268	4	258	3
J-5–24	348	167	0.48	0.1630	0.0017	10.44	0.13	0.4645	0.0058	2487	10	2474	12	2459	25
J-5–25	149	206	1.39	0.1710	0.0019	10.50	0.14	0.4453	0.0056	2568	10	2480	12	2374	25
J-5–26	66	43	0.66	0.1653	0.0019	10.32	0.14	0.4527	0.0057	2510	10	2463	12	2407	25
J-5–27	43	46	1.07	0.1583	0.0019	9.583	0.130	0.4390	0.0055	2438	10	2396	12	2346	25
J-5–29	335	89	0.27	0.1631	0.0017	10.77	0.14	0.4789	0.0060	2488	10	2504	12	2522	26
J-5–30	73	77	1.06	0.05789	0.00196	0.3553	0.0120	0.0445	0.0007	526	48	309	9	281	4
J-5–31	50	41	0.84	0.1331	0.0016	6.967	0.097	0.3796	0.0048	2140	11	2107	12	2075	22
J-5–32	436	198	0.45	0.05566	0.00202	0.3293	0.0111	0.0429	0.0006	439	83	289	9	271	4
J-5–33	715	695	0.97	0.05849	0.00271	0.3111	0.0137	0.0386	0.0006	548	104	275	11	244	3
J-5–34	171	110	0.65	0.1639	0.0018	9.190	0.118	0.4068	0.0051	2496	10	2357	12	2200	23
J-5–35	980	455	0.46	0.1663	0.0035	5.901	0.096	0.2573	0.0033	2521	36	1961	14	1476	17
J-5–36	237	169	0.71	0.05526	0.00089	0.3099	0.0054	0.0407	0.0005	423	18	274	4	257	3
J-5–37	442	207	0.47	0.05803	0.00179	0.3355	0.0094	0.0419	0.0006	531	69	294	7	265	3
J-5–38	273	109	0.40	0.1642	0.0018	11.12	0.14	0.4915	0.0061	2499	10	2534	12	2577	26
J-5–39	537	150	0.28	0.2065	0.0022	16.23	0.21	0.5698	0.0071	2879	9	2890	12	2907	29
J-5–40	190	158	0.83	0.05323	0.00097	0.2899	0.0056	0.03950	0.00050	339	22	258	4	250	3
J-5–41	60	26	0.44	0.05315	0.00175	0.2857	0.0094	0.03900	0.00056	335	49	255	7	247	3
J-5–42	260	314	1.21	0.1645	0.0018	9.784	0.128	0.4313	0.0054	2503	10	2415	12	2312	24
J-5–43	156	96	0.62	0.1662	0.0018	10.81	0.14	0.4716	0.0059	2520	10	2507	12	2491	26
J-5–44	138	140	1.02	0.06053	0.00321	0.3524	0.0179	0.04222	0.00062	623	117	306	13	267	4
J-5–46	183	98	0.54	0.1602	0.0018	10.13	0.13	0.4587	0.0058	2457	10	2447	12	2434	25
J-5–47	321	396	1.23	0.1622	0.0018	8.243	0.108	0.3686	0.0046	2479	10	2258	12	2023	22
J-5–48	330	528	1.60	0.05602	0.00085	0.3278	0.0054	0.04244	0.00054	453	17	288	4	268	3
J-5–49	320	227	0.71	0.1689	0.0019	11.40	0.15	0.4894	0.0061	2547	10	2556	12	2568	27
J-5–50	331	47	0.14	0.1138	0.0013	5.322	0.070	0.3393	0.0043	1861	11	1872	11	1883	21
J-5–51	159	127	0.80	0.1656	0.0040	10.76	0.22	0.4712	0.0065	2514	42	2503	19	2489	28
J-5–52	129	62	0.48	0.1830	0.0020	13.29	0.18	0.5268	0.0066	2680	10	2700	13	2728	28
J-5–53	217	187	0.86	0.05307	0.00082	0.3805	0.0065	0.05200	0.00070	332	18	327	5	327	4
J-5–54	155	105	0.68	0.1064	0.0012	4.598	0.062	0.3136	0.0040	1738	11	1749	11	1758	19
J-5–55	242	152	0.63	0.1601	0.0018	10.62	0.14	0.4810	0.0061	2457	10	2490	12	2532	26
J-5–56	270	206	0.76	0.1701	0.0019	10.26	0.14	0.4375	0.0055	2558	10	2458	12	2339	25
J-5–57	57	56	0.97	0.1111	0.0014	5.140	0.074	0.3355	0.0043	1818	12	1843	12	1865	21
J-5–58	663	75	0.11	0.1566	0.0029	8.782	0.117	0.4068	0.0050	2419	32	2316	12	2200	23
J-5–59	226	90	0.40	0.1685	0.0019	11.13	0.15	0.4792	0.0060	2543	10	2534	12	2524	26
J-5–60	116	53	0.46	0.1658	0.0019	11.25	0.15	0.4921	0.0062	2516	10	2544	13	2580	27
J-5–61	121	39	0.33	0.1652	0.0019	10.98	0.15	0.4819	0.0061	2510	10	2521	13	2535	26
J-5–62	733	1258	1.72	0.1696	0.0019	6.717	0.089	0.2873	0.0036	2554	10	2075	12	1628	18
J-5–63	153	46	0.30	0.1531	0.0018	9.098	0.123	0.4311	0.0055	2381	10	2348	12	2311	25
J-5–64	2021	369	0.18	0.1524	0.0017	6.514	0.086	0.3100	0.0039	2373	10	2048	12	1741	19
J-5–65	437	200	0.46	0.05340	0.00077	0.303	0.0048	0.0412	0.0005	346	16	269	4	260	3
J-5–66	174	254	1.46	0.1623	0.0019	10.19	0.14	0.4555	0.0058	2480	10	2452	13	2419	26
J-5–68	635	75	0.12	0.1651	0.0019	10.63	0.14	0.4669	0.0059	2509	10	2491	12	2470	26
J-5–69	222	222	1.00	0.0533	0.0009	0.3718	0.0065	0.05060	0.00070	342	19	321	5	318	4
J-5–70	448	189	0.42	0.1622	0.0018	9.931	0.133	0.4441	0.0056	2479	10	2428	12	2369	25
J-5–71	507	138	0.27	0.05166	0.00155	0.2972	0.0080	0.04172	0.00054	270	70	264	6	264	3
J-5–72	210	33	0.16	0.1152	0.0013	5.491	0.075	0.3456	0.0044	1883	11	1899	12	1914	21
J-5–73	348	158	0.45	0.1658	0.0019	10.79	0.15	0.4721	0.0060	2516	10	2505	13	2493	26
J-5–74	99	117	1.18	0.1693	0.0020	11.00	0.15	0.4714	0.0060	2550	10	2523	13	2490	26
J-5–75	949	507	0.53	0.0523	0.0007	0.3123	0.0046	0.04333	0.00055	297	15	276	4	273	3

(*continued on next page*)

Table 1 (*continued*)

Spots	Element (ppm)		Th/U	Isotopic ratios						Apparent age (Ma)					
	U	Th		$^{207}Pb/^{206}Pb$	1σ	$^{207}Pb/^{235}U$	1σ	$^{206}Pb/^{238}U$	1σ	$^{207}Pb/^{206}Pb$	1σ	$^{207}Pb/^{235}U$	1σ	$^{206}Pb/^{238}U$	1σ
J-5–76	144	114	0.79	0.05559	0.00100	0.3796	0.0073	0.04953	0.00065	436	21	327	5	312	4
J-5–77	525	163	0.31	0.1694	0.0019	11.51	0.16	0.4931	0.0062	2551	10	2566	13	2584	27
J-5–78	217	168	0.78	0.1656	0.0019	11.21	0.15	0.4913	0.0062	2513	10	2541	13	2576	27
J-5–79	301	165	0.55	0.1598	0.0019	10.35	0.14	0.4698	0.0060	2454	10	2467	13	2482	26
J-5–80	286	186	0.65	0.05517	0.00079	0.4750	0.0076	0.06244	0.00080	419	16	395	5	390	5
Y-1–01	676	178	0.26	0.1199	0.0013	5.707	0.067	0.3452	0.0038	1955	9	1932	10	1912	18
Y-1–02	228	145	0.64	0.1113	0.0029	4.707	0.106	0.3068	0.0037	1820	48	1768	19	1725	18
Y-1–03	3115	1286	0.41	0.05512	0.00064	0.3384	0.0042	0.04453	0.00049	417	12	296	3	281	3
Y-1–04	47	50	1.07	0.1083	0.0016	4.838	0.073	0.3240	0.0037	1771	13	1791	13	1809	18
Y-1–05	150	104	0.70	0.06529	0.00125	0.4114	0.0079	0.04569	0.00053	784	22	350	6	288	3
Y-1–06	187	42	0.22	0.1647	0.0028	10.57	0.13	0.4654	0.0051	2505	29	2486	12	2463	23
Y-1–07	68	64	0.94	0.1125	0.0014	5.275	0.068	0.3402	0.0038	1839	10	1865	11	1888	18
Y-1–08	82	43	0.53	0.1179	0.0014	5.652	0.069	0.3477	0.0039	1925	10	1924	11	1924	19
Y-1–10	657	204	0.31	0.05421	0.00134	0.3159	0.008	0.04227	0.00051	380	34	279	6	267	3
Y-1–11	152	60	0.39	0.1156	0.0012	5.480	0.063	0.3439	0.0038	1889	9	1898	10	1905	18
Y-1–12	2501	2255	0.90	0.05789	0.00064	0.3586	0.0043	0.04492	0.00049	526	12	311	3	283	3
Y-1–13	157	117	0.75	0.1157	0.0013	5.278	0.063	0.3309	0.0037	1891	10	1865	10	1843	18
Y-1–14	345	219	0.63	0.05833	0.00091	0.5518	0.0088	0.06860	0.00078	542	17	446	6	428	5
Y-1–15	154	41	0.27	0.1141	0.0013	5.208	0.062	0.3311	0.0037	1865	10	1854	10	1844	18
Y-1–16	849	415	0.49	0.04672	0.00315	0.2493	0.01653	0.03870	0.00048	35	149	226	13	245	3
Y-1–17	139	61	0.44	0.1173	0.0013	5.586	0.067	0.3455	0.0038	1915	10	1914	10	1913	18
Y-1–18	223	73	0.33	0.05509	0.00079	0.5239	0.0077	0.06898	0.00077	416	15	428	5	430	5
Y-1–19	261	92	0.35	0.1141	0.0012	5.273	0.062	0.3353	0.0037	1865	9	1865	10	1864	18
Y-1–20	76	65	0.85	0.05634	0.00127	0.4036	0.0091	0.05196	0.00062	466	29	344	7	327	4
Y-1–21	376	228	0.61	0.1128	0.0012	5.086	0.059	0.3269	0.0036	1845	9	1834	10	1823	18
Y-1–22	1086	209	0.19	0.1110	0.0012	5.084	0.058	0.3322	0.0037	1816	9	1833	10	1849	18
Y-1–23	258	63	0.25	0.1103	0.0013	4.896	0.061	0.3218	0.0036	1805	10	1802	11	1799	18
Y-1–24	488	301	0.62	0.1190	0.0013	5.890	0.068	0.3589	0.0040	1942	9	1960	10	1977	19
Y-1–25	97	47	0.48	0.1130	0.0013	5.088	0.063	0.3266	0.0036	1848	10	1834	10	1822	18
Y-1–26	203	104	0.51	0.05706	0.00081	0.5693	0.0083	0.07236	0.00081	494	15	458	5	450	5
Y-1–27	141	70	0.50	0.05166	0.00120	0.3298	0.0077	0.04630	0.00055	270	32	289	6	292	3
Y-1–28	287	81	0.28	0.1681	0.0018	11.57	0.13	0.4993	0.0055	2539	9	2570	11	2611	24
Y-1–29	1259	92	0.07	0.1154	0.0018	5.192	0.060	0.3264	0.0035	1885	29	1851	10	1821	17
Y-1–30	129	70	0.54	0.1703	0.0019	11.73	0.14	0.4996	0.0055	2561	9	2583	11	2612	24
Y-1–31	307	122	0.40	0.05133	0.00095	0.2914	0.0054	0.04117	0.00047	256	23	260	4	260	3
Y-1–32	323	206	0.64	0.1146	0.0013	5.349	0.063	0.3385	0.0037	1874	9	1877	10	1879	18
Y-1–33	21	17	0.82	0.04605	0.00381	0.3218	0.0263	0.05069	0.00071		182	283	20	319	4
Y-1–34	165	61	0.37	0.05706	0.00091	0.5677	0.0093	0.07215	0.00082	494	18	457	6	449	5
Y-1–35	231	340	1.47	0.1141	0.0013	5.287	0.063	0.3362	0.0037	1865	10	1867	10	1868	18
Y-1–36	637	51	0.08	0.1149	0.0019	5.037	0.062	0.3179	0.0035	1879	30	1826	10	1779	17
Y-1–37	47	22	0.47	0.05352	0.00171	0.3223	0.0102	0.04368	0.00057	351	48	284	8	276	4
Y-1–38	401	136	0.34	0.06332	0.00216	0.4329	0.0138	0.04958	0.00060	719	74	365	10	312	4
Y-1–39	93	60	0.65	0.1127	0.0014	5.076	0.064	0.3267	0.0037	1843	10	1832	11	1822	18
Y-1–40	121	128	1.05	0.05785	0.00102	0.4793	0.0086	0.06009	0.00069	524	20	398	6	376	4
Y-1–41	653	366	0.56	0.05411	0.00072	0.3604	0.0050	0.04831	0.00054	376	14	312	4	304	3
Y-1–42	58	41	0.71	0.05860	0.00169	0.3801	0.0108	0.04704	0.00060	552	40	327	8	296	4
Y-1–43	289	34	0.12	0.05022	0.00083	0.3096	0.0052	0.04471	0.00051	205	20	274	4	282	3
Y-1–44	477	355	0.74	0.1304	0.0015	6.922	0.083	0.3850	0.0043	2103	9	2101	11	2100	20
Y-1–45	226	69	0.31	0.1190	0.0014	6.188	0.075	0.3772	0.0042	1941	10	2003	11	2063	20
Y-1–46	379	270	0.71	0.1736	0.0019	12.09	0.14	0.5052	0.0056	2592	9	2612	11	2636	24
Y-1–47	106	41	0.38	0.1624	0.0019	10.62	0.13	0.4742	0.0053	2481	9	2490	11	2502	23
Y-1–48	123	52	0.42	0.1143	0.0013	5.459	0.068	0.3465	0.0039	1868	10	1894	11	1918	19
Y-1–49	331	602	1.82	0.05345	0.00087	0.3684	0.0062	0.04999	0.00057	348	19	318	5	314	3
Y-1–50	58	49	0.84	0.1054	0.0015	4.625	0.066	0.3184	0.0037	1721	12	1754	12	1782	18
Y-1–51	530	453	0.85	0.05173	0.00073	0.3231	0.0047	0.04530	0.00051	273	16	284	4	286	3
Y-1–52	69	104	1.51	0.07431	0.00218	0.4744	0.0137	0.04630	0.00061	1050	37	394	9	292	4
Y-1–53	265	115	0.43	0.1557	0.0031	9.542	0.154	0.4444	0.0052	2410	35	2392	15	2370	23
Y-1–54	408	298	0.73	0.05215	0.00085	0.3185	0.0053	0.04429	0.00051	292	19	281	4	279	3
Y-1–55	176	83	0.47	0.05456	0.00108	0.3385	0.0068	0.04499	0.00053	394	25	296	5	284	3
Y-1–56	1775	306	0.17	0.05520	0.00126	0.5278	0.0105	0.06935	0.00078	420	52	430	7	432	5
Y-1–57	158	82	0.52	0.1140	0.0014	5.394	0.068	0.3430	0.0039	1865	10	1884	11	1901	18
Y-1–58	970	267	0.27	0.05546	0.00071	0.5883	0.0079	0.07693	0.00086	431	14	470	5	478	5
Y-1–59	353	74	0.21	0.1175	0.0014	5.578	0.069	0.3444	0.0039	1918	10	1913	11	1908	18
Y-1–60	503	198	0.39	0.06399	0.00192	1.081	0.03	0.1226	0.0015	741	65	744	15	745	8
Y-1–61	171	117	0.68	0.1122	0.0013	5.296	0.067	0.3422	0.0038	1836	10	1868	11	1897	18
Y-1–62	158	46	0.29	0.1657	0.0032	11.026	0.171	0.4826	0.0056	2515	33	2525	14	2539	24
Y-1–63	551	331	0.60	0.05471	0.00081	0.3270	0.0050	0.04334	0.00049	400	16	287	4	274	3
Y-1–64	279	335	1.20	0.1041	0.0019	0.6854	0.0123	0.04775	0.00057	1698	17	530	7	301	4
Y-1–65	628	42	0.07	0.06584	0.00090	0.4908	0.0070	0.05406	0.00061	801	14	405	5	339	4
Y-1–66	1736	255	0.15	0.07855	0.00100	0.7672	0.0103	0.07083	0.00080	1161	12	578	6	441	5
Y-1–67	96	45	0.47	0.1520	0.0023	9.382	0.146	0.4476	0.0054	2369	12	2376	14	2384	24
Y-1–68	130	87	0.66	0.1074	0.0014	5.069	0.067	0.3422	0.0039	1756	11	1831	11	1897	19
Y-1–69	51	42	0.82	0.1581	0.0021	10.73	0.15	0.4923	0.0057	2435	10	2500	13	2580	24
Y-1–70	668	134	0.20	0.1031	0.0021	3.507	0.058	0.2468	0.0028	1680	38	1529	13	1422	15

Table 1 (*continued*)

Spots	Element (ppm)		Th/U	Isotopic ratios						Apparent age (Ma)					
	U	Th		$^{207}Pb/^{206}Pb$	1σ	$^{207}Pb/^{235}U$	1σ	$^{206}Pb/^{238}U$	1σ	$^{207}Pb/^{206}Pb$	1σ	$^{207}Pb/^{235}U$	1σ	$^{206}Pb/^{238}U$	1σ
Y-1–71	476	53	0.11	0.1155	0.0014	5.703	0.073	0.3583	0.0040	1887	10	1932	11	1974	19
Y-1–72	388	126	0.32	0.05375	0.00102	0.3354	0.0065	0.04526	0.00053	361	23	294	5	285	3
Y-1–73	110	42	0.38	0.05536	0.00147	0.5595	0.0148	0.07330	0.00092	427	37	451	10	456	6
Y-1–74	46	53	1.17	0.1636	0.0022	11.30	0.16	0.5009	0.0058	2493	11	2548	13	2618	25
Y-1–75	193	94	0.49	0.1099	0.0023	0.7726	0.0160	0.05100	0.00064	1797	20	581	9	321	4
Y-1–76	58	37	0.63	0.05563	0.00309	0.3950	0.0216	0.05149	0.00079	438	95	338	16	324	5
Y-1–77	158	72	0.46	0.05639	0.00114	0.5680	0.0116	0.07306	0.00086	468	25	457	8	455	5
Y-1–78	143	60	0.42	0.1122	0.0014	5.646	0.076	0.3651	0.0041	1835	11	1923	12	2006	20
Y-1–79	431	395	0.92	0.05618	0.00109	0.3780	0.0074	0.04880	0.00057	459	23	326	5	307	4
Y-1–80	303	91	0.30	0.1158	0.0014	5.802	0.074	0.3635	0.0041	1892	10	1947	11	1999	19

strata: one is in the Ordos basin in the center of the NCC (Y-1), the other (J-5) is at the southern end of the Taihang Mountain, in the northwest of the Henan province (Fig. 1) (Che et al., 2002). Sample Y-1 and J-5 are all quartzose sandstone, belonging to the upper part of the Late Permian formation in these two basins.

3. Analytical methods

The size of detrital zircon varies between 50 and 250 μm. Their morphology ranges from prismatic or rounded to subhedral, showing some evidence of sedimentary abrasion. Zircons were mounted in epoxy and about 1/3 of their volume polished away. No cathodoluminescence (CL) imaging was performed prior to analysis.

Zircon U–Pb dating was carried out by Laser-Ablation–Inductivity Couple Plasma Mass Spectrometry (LA–ICPMS, Agilent 7500a) at the State Key Laboratory of Geological Processes and Mineral Resources, China University of Geosciences (Wuhan). The laser-ablation system is a GeoLas 2005 equipped with a 193 nm ArF-excimer laser and a homogenizing, imaging optical system. A 30 μm spot size and 80 Hz energy density were adopted. Standard 91,500 zircons (age 1064 Ma) were used for calibration of inter element fractionation, and U, Th and Pb concentrations were determined based

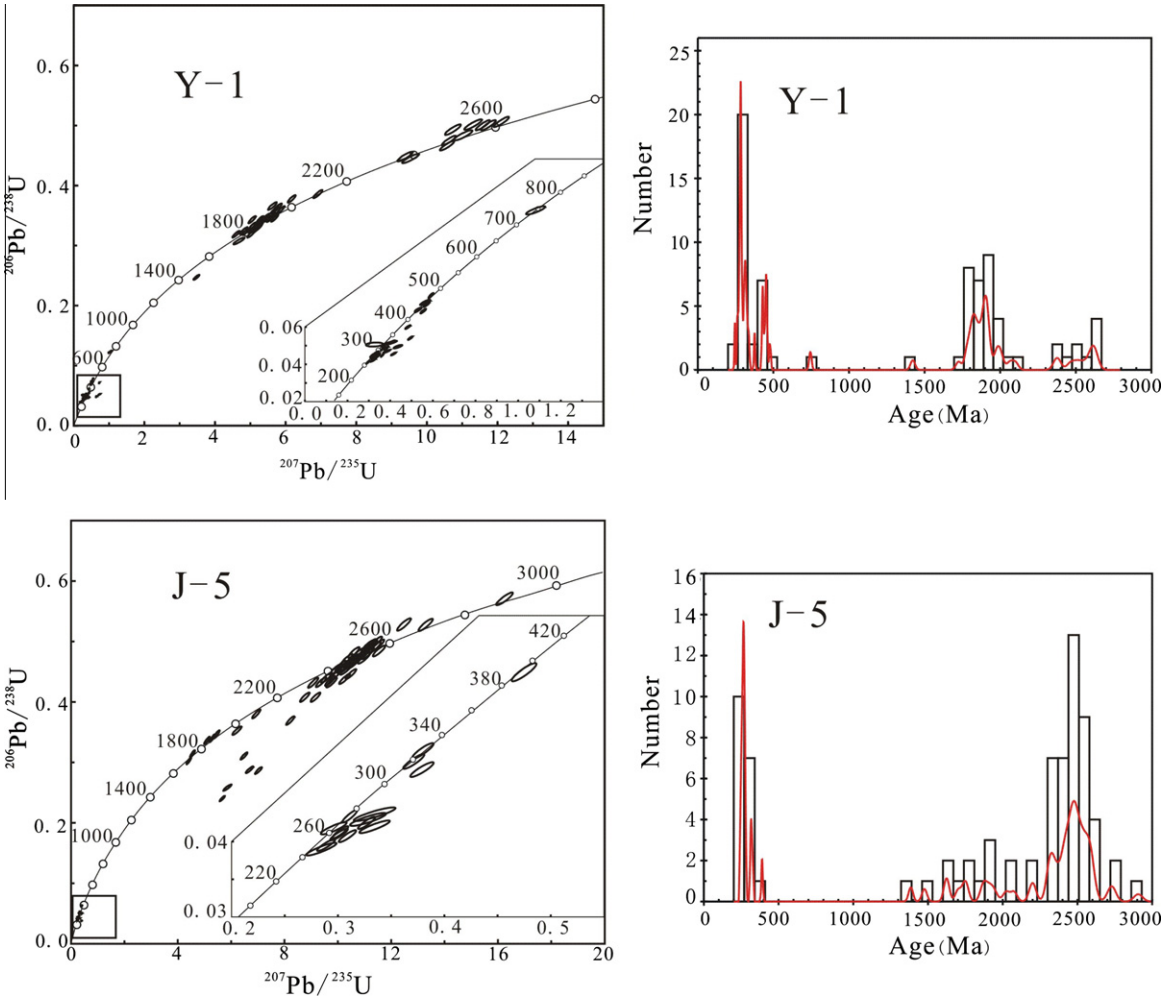

Fig. 2. Detrital zircon U–Pb concordia age diagrams and age histograms.

on the standard NIST610. The Glitter program (ver. 4.0) was used for raw data reduction and age calculation; for Pb correction the method described by Andersen (2002) was used. The age calculations and plotting of concordia diagrams were made using ISOPLOT (ver. 3.0). Detailed procedures are similar to those described by Yuan et al. (2004).

In situ Hf isotopic analyses were carried out on the spots of U–Pb age dating of Phanerozoic zircons using a Neptune MC-ICPMS, equipped with a 193 nm laser, at the Institute of Geology and Geophysics, Chinese Academy of Sciences in Beijing, China. During analyses, spot sizes of 40 μm, with a laser repetition rate of 8 Hz at 100 mJ were used. The detailed analytical technique and data correction procedure are described in Wu et al. (2007). During analyses, the $^{176}Hf/^{177}Hf$ and $^{176}Lu/^{177}Hf$ ratios of the standard zircon (91,500) were 0.282289 ± 4 ($2\sigma n$, $n = 42$) and 0.00029 respectively.

4. U–Pb ages and Hf isotopes of detrital zircons

J-5: Eighty randomly selected grains of zircons were analyzed for U–Pb ages using LA-ICP-MS (Table 1). Four analyses were discarded because of low data acquisition. Of the remaining 76 grains, 67 grains gave concordant ages at the 90% confidence level. Because of the low content of radiogenic Pb and the uncertainty associated with Pb correction, the $^{207}Pb/^{206}Pb$ age is used for samples with ages greater than 1000 Ma and the $^{206}Pb/^{238}U$ age for samples with age below 1000 Ma (Zhou et al., 2007). The 67 ages fall into three groups: 247–390 Ma (15 grains), 1738–2140 Ma (seven grains, peaked at 1850 Ma), and 2381–2879 Ma (45 grains, peaked at 2500 Ma) (Fig. 2). Most of the analyses show elevated Th/U ratios, indicating a magmatic origin. Some zircons experienced Pb loss as a consequence of interaction with low temperature fluids.

Table 2
Neptune MC-ICPMS Lu-Hf isotope analyses of detrital zircons.

Sample spot	$^{176}Yb/^{177}Hf$	$^{176}Lu/^{177}Hf$	$^{176}Hf/^{177}Hf$	±(2σ)	$^{206}Pb/^{238}U$ age (Ma)	$\varepsilon_{Hf}(t)$	±(2σ)	T_{DM} (Ma)	±(2σ)
J-5–12	0.016773	0.000660	0.282403	0.000021	275	−7.1	0.7	1.19	0.03
J-5–23	0.018545	0.000721	0.282370	0.000023	258	−8.7	0.8	1.24	0.03
J-5–30	0.018404	0.000745	0.282210	0.000023	281	−13.9	0.8	1.46	0.03
J-5–32	0.034065	0.001378	0.282335	0.000017	271	−9.8	0.6	1.31	0.02
J-5–33	0.049706	0.001918	0.282327	0.000019	244	−10.7	0.7	1.34	0.03
J-5–36	0.031098	0.001263	0.282217	0.000019	257	−14.2	0.7	1.47	0.03
J-5–37	0.072166	0.002348	0.282377	0.000019	265	−8.6	0.7	1.28	0.03
J-5–40	0.020094	0.000794	0.282768	0.000018	250	5.2	0.7	0.68	0.03
J-5–41	0.009385	0.000345	0.282583	0.000020	247	−1.3	0.7	0.93	0.03
J-5–44	0.021073	0.000868	0.282225	0.000023	267	−13.7	0.8	1.44	0.03
J-5–48	0.037038	0.001587	0.282161	0.000019	268	−16.0	0.7	1.56	0.03
J-5–53	0.031628	0.001238	0.282215	0.000018	327	−12.8	0.6	1.47	0.03
J-5–65	0.029816	0.001237	0.282293	0.000019	260	−11.5	0.7	1.36	0.03
J-5–69	0.027716	0.001115	0.282369	0.000019	318	−7.5	0.7	1.25	0.03
J-5–71	0.019211	0.000840	0.282463	0.000019	264	−5.3	0.7	1.11	0.03
J-5–75	0.040345	0.001637	0.282424	0.000020	273	−6.6	0.7	1.19	0.03
J-5–76	0.017064	0.000792	0.282179	0.000020	312	−14.3	0.7	1.50	0.03
J-5–80	0.026855	0.001198	0.281784	0.000020	390	−26.7	0.7	2.07	0.03
Y-1–03	0.082540	0.002881	0.282322	0.000019	281	−10.3	0.7	1.38	0.03
Y-1–05	0.029838	0.001188	0.282127	0.000020	288	−16.7	0.7	1.59	0.03
Y-1–10	0.022419	0.000922	0.282125	0.000023	267	−17.2	0.8	1.58	0.03
Y-1–12	0.076699	0.002760	0.282337	0.000020	283	−9.7	0.7	1.35	0.03
Y-1–14	0.024228	0.001125	0.282731	0.000021	428	7.7	0.8	0.74	0.03
Y-1–16	0.020842	0.000809	0.282372	0.000017	245	−8.9	0.6	1.24	0.02
Y-1–18	0.011542	0.000478	0.282201	0.000020	430	−10.9	0.7	1.46	0.03
Y-1–20	0.019679	0.000732	0.282470	0.000017	327	−3.6	0.6	1.10	0.02
Y-1–26	0.017706	0.000833	0.282550	0.000019	450	1.8	0.7	0.99	0.03
Y-1–27	0.024242	0.000868	0.282486	0.000019	292	−3.9	0.7	1.08	0.03
Y-1–31	0.027094	0.001061	0.282328	0.000017	260	−10.2	0.6	1.31	0.02
Y-1–33	0.024740	0.000996	0.282250	0.000029	319	−11.7	1.0	1.41	0.04
Y-1–36	0.019127	0.000660	0.281499	0.000016	1879	−3.9	0.6	2.43	0.02
Y-1–37	0.025497	0.001007	0.282232	0.000021	276	−13.2	0.7	1.44	0.03
Y-1–38	0.098301	0.003094	0.282548	0.000028	312	−1.7	1.0	1.05	0.04
Y-1–40	0.018817	0.000745	0.282009	0.000018	376	−18.9	0.6	1.74	0.02
Y-1–41	0.046969	0.001654	0.282489	0.000017	304	−3.7	0.6	1.10	0.02
Y-1–42	0.022290	0.000878	0.282196	0.000026	296	−14.0	0.9	1.48	0.04
Y-1–43	0.006990	0.000255	0.282279	0.000017	282	−11.3	0.6	1.35	0.02
Y-1–49	0.063440	0.002461	0.282339	0.000022	314	−8.9	0.8	1.34	0.03
Y-1–51	0.075834	0.002694	0.282295	0.000023	286	−11.1	0.8	1.41	0.03
Y-1–54	0.042863	0.001507	0.282550	0.000021	279	−2.0	0.7	1.01	0.03
Y-1–55	0.047300	0.001730	0.282839	0.000021	284	8.3	0.7	0.60	0.03
Y-1–56	0.036829	0.001266	0.282274	0.000020	432	−8.5	0.7	1.39	0.03
Y-1–58	0.035769	0.001275	0.282294	0.000019	478	−6.8	0.7	1.36	0.03
Y-1–60	0.057080	0.001873	0.282141	0.000023	745	−6.8	0.8	1.60	0.03
Y-1–63	0.056699	0.001977	0.282650	0.000022	274	1.4	0.8	0.87	0.03
Y-1–65	0.035438	0.001293	0.282302	0.000022	339	−9.5	0.8	1.35	0.03
Y-1–72	0.033843	0.001116	0.282456	0.000020	285	−5.1	0.7	1.13	0.03
Y-1–73	0.015553	0.000574	0.282621	0.000021	456	4.5	0.7	0.88	0.03
Y-1–76	0.032260	0.001158	0.282233	0.000021	324	−12.2	0.7	1.44	0.03
Y-1–77	0.018248	0.000706	0.282551	0.000021	455	2.0	0.7	0.98	0.03
Y-1–79	0.028242	0.001029	0.282104	0.000018	307	−17.1	0.6	1.62	0.02

Initial Hf isotope ratios are calculated with reference to the chondritic reservoir at the time of magma crystallization, a decay constant for ^{176}Lu of 1.867×10^{-11} a^{-1} (Soderlund et al., 2004) and chondritic ratios of $^{176}Hf/^{177}Hf$ (=0.282772) and $^{176}Lu/^{177}Hf$ (=0.0332) (Blichert-Toft and Albarede, 1997) were adopted. Single-stage model ages (T_{DM}) are calculated using the measured $^{176}Lu/^{177}Hf$ ratios, referring to a model depleted mantle with a present-day $^{176}Hf/^{177}Hf$ ratio of 0.28325 and $^{176}Lu/^{177}Hf = 0.0384$ (Griffin et al., 2000). The crystallization ages are the single zircon U–Pb ages analyzed above.

The youngest zircon age (247 ± 3 Ma) is only slightly younger than the real depositional age of the Formation. *In situ* Lu–Hf isotope analyses were carried out on zircons of group 1. The results yield $^{176}Hf/^{177}Hf$ ratios from 0.281784 to 0.282768 and corresponding $\varepsilon_{Hf}(t)$ values from −1.3 to −26.7 for most of the zircons but one grain gave a value of 5.2 (Fig. 4). The Hf isotopic model ages (T_{DM}) for these zircons range from 0.66 to 2.04 Ga (Table 2).

Y-1: As for sample J-5, 80 randomly selected grains of zircons were analyzed for U–Pb ages. One analysis was discarded. We obtained 79 U–Pb ages from 79 zircon grains, of which 72 were

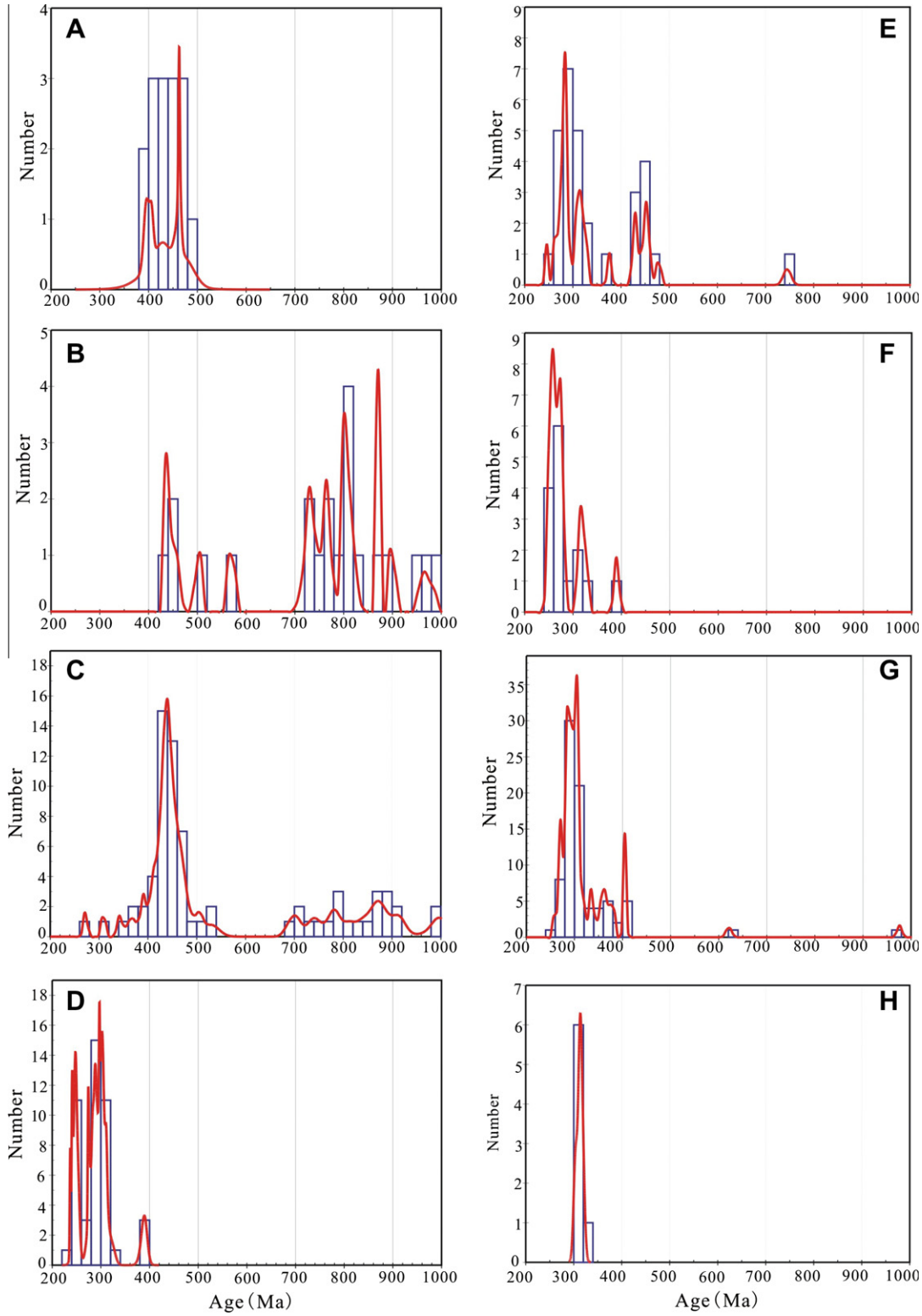

Fig. 3. Age histogram of Late Paleozoic detrital zircons of sedimentary formation around the NCC. (A) Northern Qinling Orogen igneous rocks (Ma et al., 2004; Jiang et al., 2005; and references therein). (B) Quartzite samples of the Foziling complex from the northern Dabie Orogen (Chen et al., 2003). (C) Carboniferous sediments from northern Dabie Orogen (Li et al., 2004). (D) Inner Mongolia Paleo-uplift igneous rocks (Zhang et al., 2006, 2007a–c, 2009; Zhao et al., 2007). (E) Sample Y-1. (F) Sample J-5. (G). Late Paleozoic sediments of the Xishan basin (Yang et al., 2006). (H). Carboniferous sediments from the Ningwu-Jingle basin (Li et al., 2009).

concordant at the 90% confidence level. The 72 analyses fall into four groups: 245–376 Ma (21 grains), 428–745 Ma (nine grains), 1680–1941 Ma (29 grains, peaked at 1850 Ma), and 2103–2592 Ma (13 grains, peaked at 2500 Ma) (Fig. 2). Their Th/U ratios indicate that the grains are magmatic. The youngest zircon age (245 ± 3 Ma) is close to depositional age of the Formation. The $^{176}Hf/^{177}Hf$ ratios of zircons from the first two groups range from 0.282009 to 0.282839 and corresponding $\varepsilon_{Hf}(t)$ values are from −18.9 to 8.3 (Fig. 4). The Hf isotopic model ages (T_{DM}) for these zircons range from 0.66 to 2.04 Ga (Table 2).

5. Provenance analyses of detrital zircons

5.1. Source characteristics of different tectonic units

The hinterland of the NCC, the Xing-Meng Orogenic Belt, the Inner Mongolia Paleo-uplift, the Northern Qinling Orogen, the Southern Qinling Orogen, the Dabie Orogen, and the Yangze plate all constitute potential sedimentary sources for the NCC during the Paleozoic. Determining the provenance from these tectonic units is the impetus for our study.

The NCC is characterized by Neoarchean and Paleoproterozoic basement (Zhao et al., 2001; Chen et al., 2003; Li et al., 2004; Derby and Gehrels, 2006; Wu et al., 2008) whereas the Yangtze plate exhibits Neoproterozoic magmatic activity (Chen et al., 2003; Li et al., 2004). The Northern Qinling Orogen is characterized by Early Paleozoic igneous rocks whereas the Southern Qinling Orogen is characterized by rocks with signatures of Yangtze plate basement and cover rocks without any Early Paleozoic magmatism. The Early Paleozoic igneous rocks of the Northern Qinling Orogen were derived from both continental crust and depleted mantle sources (i.e. double-peak in $\varepsilon_{Nd}(t)$ values). Many scholars regard the Early Paleozoic zircon U–Pb ages as the diagnostic feature of the Northern Qinling Orogen provenance (Ma et al., 2004). Although the northern Dabie Orogen corresponds geographically to the eastern segment of the Northern Qinling Orogen, its eastern segment is composed mainly of Neoproterozoic Luzhenguan group granitic gneiss and amphibolite (700–800 Ma), Early Paleozoic-Devonian Foziling group terrigenous debris, alternating with Carboniferous marine-land facies coal-bearing shale and sandstone, correspond to Southern Qinling Orogen in geochemical characteristics.

Late Paleozoic magmatic activity within the NCC occurs mainly in the Inner Mongolia Paleo-uplift and is of Andean type. The Xing-Meng Orogenic Belt, which is north of the NCC, is a typical Phanerozoic complex Orogenic belt formed by successive accretion of arc complexes, accompanied by emplacement of voluminous lavas and granitic magmas from Paleozoic to Mesozoic age (Wu et al., 2000, 2001, 2002, 2003a,b). U–Pb ages of the Phanerozoic zircons from the Inner Mongolia Paleo-uplift range from 395 to 107 Ma, with mainly negative $\varepsilon_{Hf}(t)$ values except for an extremely few zircons with positive values that come from mafic–ultramafic complexes (Zhang et al., 2009). In sharp contrast, U–Pb ages of zircons from the Xing-Meng Orogenic Belt igneous rocks are all Phanerozoic, ranging from 531 to 111 Ma, with $\varepsilon_{Hf}(t)$ values of −4.2 to 16.3 (Yang et al., 2006; Li et al., 2009; Zhang et al., 2009).

5.2. Detrital zircon provenance analyses

The analyses of the two samples were divided into three groups based on their U–Pb ages: Phanerozoic, Paleoproterozoic, and Neoarchean. The Paleoproterozoic and Neoarchean zircons do not provide unambiguous information about the cratonic edges because they could come from the erosion of the craton basement or have been recycled from earlier sediments. The Phanerozoic zircons, on the other hand, may preserve information from the sedimentary source rocks and be used to infer paleogeography movement because they originate from the craton's margin or from external sources (Li et al., 2005, 2009; Yang et al., 2006).

Provenances of the group 1 zircons from the two samples are discussed together in view of their similar U–Pb ages and Hf isotopes. Forty-two analyses (245–390 Ma) yielded negative $\varepsilon_{Hf}(t)$ values ranging from −1.3 to −26.7, whereas only three analyses yielded positive $\varepsilon_{Hf}(t)$ values (1.4, 5.2 and 8.3) (Fig. 3 and 4). In terms of their crystallization ages and Hf isotope compositions, most of these zircons are very similar to the known Late Paleozoic igneous zircons from the Inner Mongolia Paleo-uplift, but differ significantly from those of Xing-Meng Orogenic Belt. The age youngest zircon from each sample lies within error of the stratigraphic age of the sample formation, implying that these Phanerozoic zircons were embedded in these sandstones. In addition, Late Paleozoic igneous rocks in the NCC are primarily distributed in the Inner Mongolia Paleo-uplift (Zhang et al., 2006; Zhao et al., 2007). We therefore infer that the detrital zircons of the group 1 zircons in the two samples mainly came from Inner Mongolia Paleo-uplift. The provenances of the three zircons with positive $\varepsilon_{Hf}(t)$ values may be very rare mafic–ultramafic complexes in the Inner Mongolia Paleo-uplift (Zhang et al., 2009) or some small arc complexes at the northern margin of the NCC. The paleocurrent in the area from Baode County in Shanxi Province to Fugu County in Shaanxi Province was north to south trending during the Late Paleozoic, which provide important evidence for the transport of materials from the Inner Mongolia Paleo-uplift to the NCC during the Late Paleozoic (Li et al., 2009).

Seven analyses of Y-1 samples yielded Early Paleozoic ages (group 2), with $\varepsilon_{Hf}(t)$ values range from −10.9 to 7.7 (Figs. 3 and 4). The Early Paleozoic crystallization age and double-peak in $\varepsilon_{Hf}(t)$ values indicate that these zircons could come from the Northern Qinling Orogen rather than from the Inner Mongolia Paleo-uplift or the Xing-Meng Orogenic Belt. Yang et al. (2006) and Li et al. (2009) analyzed the provenance of detrital zircons from the Late Paleozoic sandstones in the Xishan and the Ningwu-Jingle basins in the northern NCC. All Phanarozoic aged zircons from those basins are Late Paleozoic and were derived from the Inner Mongolia Paleo-uplift. No Early Paleozoic zircons were found in those basins, which indicates that the Inner Mongolia Paleo-uplift and Xing-Meng Orogenic Belt did not supply Early Paleozoic zircons to the NCC, supporting the inference made earlier that the Early Paleozoic zircons of sample Y-1 came from the Northern Qinling Orogen.

Detrital zircon provenance analyses of Late Paleozoic sandstones of the NCC confirm the aforementioned the Late Paleozoic elevation of the Inner Mongolia Paleo-uplift, and western part of

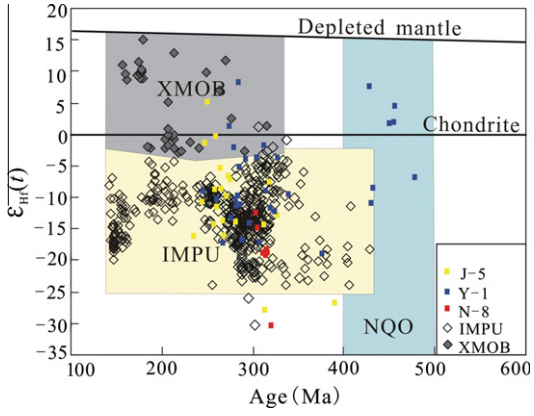

Fig. 4. Hf isotopes of detrital zircons. Cited data of the Inner Mongolia Paleo-uplift and Xing-Meng Orogenic Belt are from literature (Yang et al., 2006; Wang et al., 2009; Zhang et al., 2009a,b).

Southern Qinling Orogen, relative to the center of the craton (Fig. 5).

6. Discussion

Subduction of oceanic plates underneath both the southern and northern margins of the NCC created two continental magmatic arc belts during the Paleozoic, one at the Northern Qinling Orogen during the Early Paleozoic (before 400 Ma) (Lerch et al., 1996a,b; Meng and Zhang, 1999; Li et al., 2001), the other at the Inner Mongolia Paleo-uplift during the Late Paleozoic (after 400 Ma) (Xiao et al., 2003; Zhang et al., 2007a). The response of the NCC to these plate interactions has not been well constrained because of the deep emplacement of those intrusions and the lack of contemporaneous volcanic rocks related to the two arc belts (Zhang et al., 2006). Detrital zircon provenance analyses provide important constraints on plate kinematics (Li et al., 2004, 2005, 2009; Yang et al., 2006).

6.1. The southern margin of the NCC

6.1.1. Previous study

Accretion between the NCC and the Yangze plate had been envisaged as a prolonged and complex interaction (Meng and Zhang, 1999; Chen et al., 2003; Li et al., 2004). The Northern Qinling Orogen was an active continental margin and developed an Early Paleozoic arc-trench which can be traced to the western part of the Northern Dabie Orogen. It shows that subduction of the proto-Tethyan Qinling Ocean starts in the Ordovician (Lerch et al., 1996a,b; Li et al., 2001). The Southern Qinling Orogen accreted to the Northern Qinling Orogen along the Shangdan suture zone coeval with rifting away from the Yangtze plate during the Middle Silurian–Devonian, remained separated from the Yangtze plate during the Carboniferous-Permian by the Paleo-Tethyan Ocean, and was finally accreted with the Yangtze plate along the Mianlue suture zone during Late Triassic-Early Jurassic (Zhu et al., 1998; Meng and Zhang, 1999).

The quartzitic schist of the Foziling complex (Ordovician–Devonian sediments), in the northern Dabie area, contains abundant detrital zircons of Archean to Paleozoic age, with clusters at 2.5 Ga (~17%), 1.9–1.8 Ga (~30%), 1.0–0.7 Ga (~43%), and 0.5–0.4 Ga (~10%), suggesting a mixed sedimentary provenance consisting of the NCC, Northern Qinling Orogen, and Southern Qinling Orogen (Chen et al., 2003). It is suggested that the Southern Qinling Orogen must have drifted away from the Yangtze plate and been placed against the Northern Qinling Orogen before Devonian (Meng and Zhang, 1999). A few 0.5–0.4 Ga (~10%) zircons indicate that the denudation of the arc-trench was limited before Devonian.

Although many scholars favor a rough correlation between the northern Dabie belt and the Northern Qinling Orogen, no Early Paleozoic magmatism has been discovered in eastern Dabie (Jiang et al., 2005). The question whether the Early Paleozoic igneous rocks were totally denudated, or the Early Paleozoic arc-trench did not stretch to the eastern part of the Northern Dabie belt, remains to be answered.

6.1.2. Evolution of the southern margin

Phanerozoic zircons of Carboniferous-Permian sandstones from the Ningwu-Jingle (Li et al., 2009), Xishan (Yang et al., 2006), and Jiyuan basins are all Late Paleozoic and came from the Inner Mongolia Paleo-uplift. Analyses of the Permian samples from the Ordos study area, which is more remote from the Southern Qinling Orogen than the Jiyuan basin, show an increase of ~10% (similar to the percentage in the Foziling complex) of one group of Early Paleozoic ages. Detrital zircons of the Carboniferous sediments from the northern Dabie area are mainly Ordovician–Devonian (~50%), characteristic Neoproterozoic (~40%), and rarely Neoarchean-

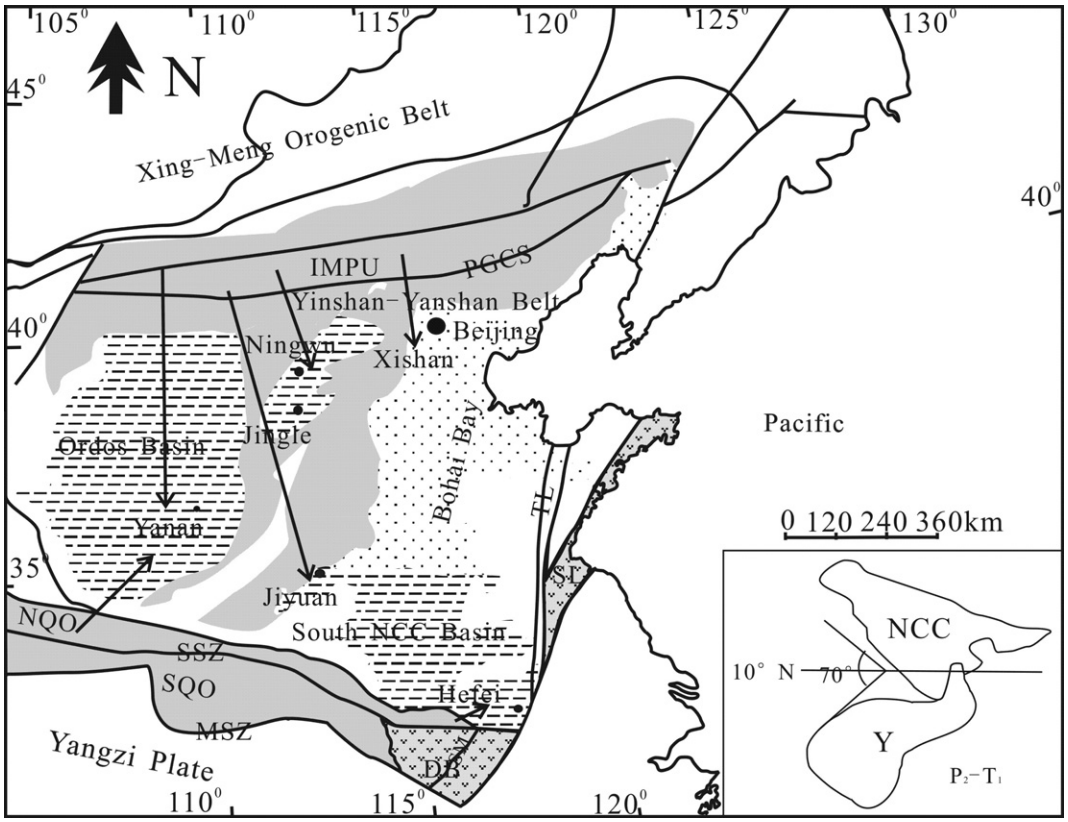

Fig. 5. Sediment source tracing model of the NCC during the Late Paleozoic.

Paleoproterozoic (~10%) (Fig. 4). These detrital zircon records indicate that there were clear differences between the evolutionary history of the Dabie Orogen, and the eastern and western Qinling Orogen. Early Paleozoic zircons only appeared in the samples of the northern Dabie area (Chen et al., 2003) and the Ordos, illustrating that the degree of elevation and denudation of the Northern Qinling Orogen was smaller during the Late Paleozoic. Many Early Paleozoic zircons occur in the northern Dabie area indicative of a strong uplift of the eastern part of the Dabie Orogen during the Carboniferous.

Paleomagnetic studies by Zhu et al. (1998) concluded that the Yangtze plate collided with the eastern NCC during Late Paleozoic and then rotated counterclockwise relative to the NCC and finally collided with the NCC during Late Triassic-Early Jurassic at the southern margin of the NCC. Although the Early Paleozoic arc-trench, which stretched to the western part of the Northern Dabie belt, has been well documented, the Northern Qinling Orogen gradually narrowed from west to east extending to the east of Nanyang Basin. It is inferred that the Early Paleozoic arc-trench was mainly located at the western part of the Northern Qinling Orogen. Its size gradually decreased from the eastern part of the Northern Qinling Orogen to the northern Dabie Orogen. Strong collision and subsequent counterclockwise rotation induced violent uplift and denudation of the Dabie Orogen during the Late Paleozoic. The residual batholith of the Early Paleozoic arc-trench at the eastern part of the northern Dabie Orogen was ultimately thrust under the NCC.

6.2. The northern margin of the NCC

Derby and Gehrels (2006) analyzed detrital zircons from the Upper Proterozoic to Ordovician strata collected from the north-central NCC. U–Pb ages of 250 single detrital zircons range from 1.72 to 2.97 Ga, indicating that the center and edges of the NCC were stable before Ordovician because all analyses yielded NCC basement ages. The emergence of Phanerozoic zircons in sediments of the northern NCC apparently started no earlier than Late Carboniferous (Li et al., 2009).

Sedimentary sources of the Ordos, Ningwu-Jingle, Jiyuan, and Xishan basins come from the Inner Mongolia Paleo-uplift during the Late Paleozoic. The Inner Mongolia Paleo-uplift supplied sediments to the entire craton during the Late Paleozoic. The youngest zircon in every sample is close to the depositional age of the strata, indicating a strong tectono-magmatic activity in Carboniferous-Permian during the Inner Mongolia Paleo-uplift.

Although most of the Late Paleozoic intrusions are deeply burrowed and no Late Paleozoic volcanic rocks were found at the northern margin of the NCC (Zhang et al., 2006, 2007a–c), numerous Late Paleozoic magmatic zircons occur in the contemporary sandstones of the inner NCC. We therefore infer that the Paleozoic zircons in the Late Paleozoic sediments of the NCC are the fingerprint of eroded volcanic rocks or of intrusions that eroded rapidly after emplacement. A tectonic scenario in which the northern margin of the NCC was uplifted strongly because of subduction of the Paleo-Asian Ocean is undeniable.

Obviously, the Inner Mongolia Paleo-uplift was activated during the Late Paleozoic. The northern margin of the NCC transformed cratonic to an active margin. Subsequent asthenospheric upwelling and lithospheric thinning of the Inner Mongolia Paleo-uplift and Liaodong Peninsula (Eastern NCC) are well documented (Yang and Li, 2008; Zhang et al., 2009). It has been shown that the destruction of the NCC was not transitory, but inhomogeneous in time and space (Menzies et al., 2007; Xu, 2007). It evolved slowly in four stages, a beginning, development, climax, and end stage during which edges to the inner craton were eroded by spreading (Xu et al., 2009). The activation of the Inner Mongolia Paleo-uplift during the Late Paleozoic represents, in all likelihood, the start of the NCC destruction.

7. Conclusions

On the basis of U–Pb dating and Hf isotope analyses on detrital zircons from the Ordos and Jiyuan Basins, the following conclusions can be drawn with respect to sediment provenance and interactions of the NCC with surrounding plates during the late Paleozoic.

(1) Three major age groups (Phanerozoic, Paleoproterozoic, and Neoarchean) are observed in detrital zircons, with the youngest grain in every sample being only slightly younger than the real depositional age of the strata. The Phanerozoic zircons from the Jiyuan basin (244–390 Ma) have $\varepsilon_{Hf}(t)$ ranging from −30.3 to −1.3, suggesting a provenance from the Inner Mongolia Paleo-uplift. A bi-modal distribution in ages and $\varepsilon_{Hf}(t)$ is noted for detrital zircons from the Ordos basin, with one resembling that for the Jiyuan basin and the other characterized by Early Paleozoic ages and relatively higher $\varepsilon_{Hf}(t)$ values (−10.9 to 7.7). A hybrid source is thus inferred for the Ordos sediments, one source being the Inner Mongolia Paleo-uplift and the other the Northern Qinling Orogen.
(2) The data presented in this paper provides new constraints on the complicated accretion of the Yangtze plate to the NCC. An elevation occurred of the western part of the Northern Qinling Orogen, relative to the eastern and central part of the craton, during Late Paleozoic. The Early Paleozoic arc-trench at the north of the Dabie Orogen may have been thrusted under the NCC by subduction of the Yangtze plate during Late Paleozoic.
(3) The Inner Mongolia Paleo-uplift was uplifted strongly during of subduction of the Paleo-Asian Ocean and functioned as a sediment source for the inner craton during the Late Paleozoic. The activation of the lithosphere of northern margin of the NCC started no later than Late Paleozoic.

Acknowledgements

This paper benefits discussions with Prof. Bernard de Jong and Zhang Shuan-hong and Ian Campbell for improving the text. We would like to express our sincere appreciation to Prof. Liu Y.-S., Dr. Zong K.-Q. and Dr. Xie L.-W. for their help during U–Pb dating and Hf isotope analyses. We also thank two anonymous reviewers for their constructive comments. We acknowledge the National Science Foundation of China (Grants 90714001, 40673038 and 40573015) and the CAS/SAFEA International Partnership Program for Creative Research Teams (KZCX2-YW-Q04-06). This is contribution No. IS – 1189 from GIGCAS.

References

Andersen, T., 2002. Correction of common lead in U–Pb analyses that do not report ^{204}Pb. Chemical Geology 192, 59–79.
Blichert-Toft, J., Albarede, F., 1997. The Lu–Hf isotope geochemistry of chondrites and the evolution of the mantle–crust system. Earth and Planetary Science Letters 148 (1–2), 243–258.
Bodet, F., Scharer, U., 2000. Evolution of the SE-Asian continent from U–Pb and Hf isotopes in single grains of zircon and baddeleyite from large rivers. Geochimica et Cosmochimica Acta 64 (12), 2067–2091.
Bruguier, O., Lancelot, J.R., Malavieille, J., 1997. U–Pb dating on single detrital zircon grains from the Triassic Songpan-Ganze flysch (Central China): provenance and tectonic correlations. Earth and Planetary Science Letters 152 (1–4), 217–231.
Che, Z.-C., Liu, L., Luo, J.-H., 2002. The Regional Tectonics of China and its Neighbors. Science Press, Beijing. pp. 31–38 (in chinese).
Chen, F., Guo, J.-H., Jiang, L.-L., Siebel, W., Cong, B.-L., Satir, M., 2003. Provenance of the Beihuaiyang lower-grade metamorphic zone of the Dabie ultrahigh-

pressure collisional Orogen, China: evidence from zircon ages. Journal of Asian Earth Sciences 22 (4), 343–352.
Davis, G.A., Zheng, Y.-D., Wang, C., Darby, B.-J., Zhang, C.-H., 2001. Mesozoic tectonic evolution of the Yanshan fold and thrust belt, with emphasis on Hebei and Liaoning Provinces, northern China. In: Hendrix, M.S., Davis, G.A. (Eds.), Paleozoic and Mesozoic Tectonic Evolution of Central Asia: From Continental Assembly to Intracontinental Deformation, vol. 194. Geological Society of America Memoir, pp. 171–198.
Derby, B.-J., Gehrels, G., 2006. Detrital zircon reference for the North China block. Journal of Asian Earth Sciences 26, 637–648.
Fan, W.M., Menzies, M.A., 1992. Destruction of aged lower lithosphere and accretion of asthenosphere mantle beneath eastern China. Geotectonica et Metallogenia 16, 171–180.
Gao, S., Rudnick, R.-L., Yuan, H.-L., Liu, X.-M., Liu, Y.-S., Xu, W.-L., Ling, W.-L., Ayers, J., Wang, X.-C., Wang, Q.-H., 2004. Recycling lower continental crust in the North China craton. Nature 432, 892–897.
Griffin, W.L., O'Reilly, S.Y., Ryan, C.G., 1992. Composition and thermal structure of the lithosphere beneath South Africa, Siberia and China: porton microprobe studies. In: Abstract of the International Symposium on Cenozoic Volcanic Rocks and Deep-seated Xenoliths of China and its Environs, Beijing, pp. 65–66.
Griffin, W.L., Pearson, N.J., Belousova, E., Jackson, S.E., van Achterbergh, E., O'Reilly, S.Y., Shee, S.R., 2000. The Hf isotope composition of cratonic mantle: LAM-MC-ICPMS analysis of zircon megacrysts in kimberlites. Geochimica et Cosmochimica Acta 64 (1), 133–147.
He, B., Xu, Y.G., Chung, S.-L., Xiao, L., Wang, Y.-M., 2003. Sedimentary evidence for a rapid, kilometer-scale crustal doming prior to the eruption of the Emeishan flood basalts. Earth and Planetary Science Letters 213 (3–4), 391–405.
He, B., Xu, Y.G., Huang, X.L., Luo, Z.Y., Shi, Y.R., Yang, Q.J., Yu, S.Y., 2007. Age and duration of the Emeishan flood volcanism, SW China: geochemistry and SHRIMP zircon U–Pb dating of silicic ignimbrites, post-volcanic Xuanwei formation and clay tuff at the Chaotian section. Earth and Planetary Science Letters 255, 306–323.
Jiang, L.-L., Wolfgang, S., Chen, F., Liu, Y.-C., Chu, D.-R., 2005. U–Pb zircon ages for the Luzhenguan complex in northern part of the eastern Dabie orogen. Science in China Series D: Earth Science 48 (9), 1357–1367.
Kinny, P.D., Maas, R., 2003. Lu-Hf and Sm–Nd isotope systems in zircon. Reviews in Mineralogy and Geochemistry 53, 327–341.
Lerch, M.F., Xue, F., Kroner, A., Todt, W., 1996a. A middle silurian early devonian magmatic arc in the Qinling mountains of central China: a reply. Journal of Geology 104 (4), 504–505.
Lerch, M.F., Xue, F., Kroner, A., Todt, W., 1996b. Early Paleozoic Island arc accretion to the North China craton and the Shang Dan fault zone: a major paleoplate boundary in eastern Asia. Journal of Geophysical Research-Solid Earth 101, 17813–17826.
Li, S.G., Huang, F., Nie, Y.H., Han, W.L., Long, G., Li, H.M., Zhang, S.Q., Zhang, Z.H., 2001. Geochemical and geochronological constraints on the suture location between the North and South China blocks in the Dabie Orogen, central China. Physics and Chemistry of the Earth Part a – Solid Earth and Geodesy 26 (9–10), 655–672.
Li, R.-W., Li, S.-Y., Jin, F.-Q., Wang, Y.S., Zhang, S.K., 2004. Provenance of carboniferous sedimentary rocks in the northern margin of Dabie mountains, central China and the tectonic significance: constraints from trace elements, mineral chemistry and SHRIMP dating of zircons. Sedimentary Geology 166 (3–4), 245–264.
Li, R.W., Wan, Y.S., Cheng, Z.Y., Zhou, J.X., Li, S.Y., Jin, F.Q., Meng, Q.G., Li, Z., Jiang, M.S., 2005. Provenance of Jurassic sediments in the Hefei basin, east-central China and the contribution of high-pressure and ultrahigh-pressure metamorphic rocks from the Dabie Shan. Earth and Planetary Science Letters 231 (3–4), 279–294.
Li, H.-Y., Xu, Y.-G., Huang, X.-L., He, B., Yan, B., 2009. Activation of northern margin of the North China Craton in Late Paleozoic: evidence from U–Pb dating and Hf isotopes of detrital zircons from the upper carboniferous Taiyuan formation in the Ningwu-Jingle basin. Chinese Science Bulletin 54 (4), 677–686.
Ma, C.Q., Ming, H.L., Yang, K.G., 2004. An Ordovician magmatic arc at the northern foot of Dabie mountains: evidence from geochronology and geochemistry of intrusive rocks. Acta Petrologica Sinica 20 (3), 393–402 (in Chinese with English abstract).
Mao, J.-W., Wang, Y.-T., Zhang, Z.-H., Yu, J.-J., Niu, B.-G., 2003. Geodynamic settings of Mesozoic large-scale mineralization in North China and adjacent areas – implication from the highly precise and accurate ages of metal deposits. Science in China Series D: Earth Sciences 23 (3–4), 125–152.
Meng, Q.-R., Zhang, G.-W., 1999. Timing of collision of the North and South China blocks: controversy and reconciliation. Geology 27 (2), 123–126.
Menzies, M.A., Fan, W.M., Zhang, M., 1993. Palaeozoic and Cenozoic lithoprobe and the loss of >120 km of Archean lithosphere, Sino-Korean craton, China. In: Prichard, H.M., Alabaster, T., Harris, N.B.W., Neary, C.R. (Eds.), Magmatic Processes and Plate Tectonic, vol. 76. Geological Society (Special Publications), pp. 71–81.
Menzies, M.A., Xu, Y.-G., Zhang, H.-F., Fan, W.-M., 2007. Integration of geology, geophysics and geochemistry: a key to understanding the North China Craton. Lithos 96 (1–2), 1–21.
Richards, A., Argles, T., Harris, N., Parrish, R., Ahmad, T., Darbyshire, F., Draganits, E., 2005. Himalayan architecture constrained by isotopic tracers from clastic sediments. Earth and Planetary Science Letters 236 (3–4), 773–796.
Soderlund, U., Patchett, P.J., Vervoort, J.D., Isachsen, C.E., 2004. The ^{176}Lu decay constant determined by Lu–Hf and U–Pb isotope systematics of Precambrian mafic intrusions. Earth and Planetary Science Letters 219 (3–4), 311–324.
Wang, F., Chen, F.-K., Hou, Z.H., Peng, P., Zhai, M.-G., 2009. Zircon ages and Sr–Nd–Hf isotopic composition of late Paleozoic granitoids in the Chongli–Chicheng area, northern margin of the North China block. Acta Petrologica Sinica 25 (11), 3057–3074 (in Chinese with English abstract).
Wu, Y.-B., Zheng, Y.-F., 2004. Genesis of zircon and its constraints on interpretation of U–Pb age. Chinese Science Bulletin 49 (15), 1554–1569.
Wu, F.Y., Jahn, B.M., Wilde, S., Sun, D.Y., 2000. Phanerozoic crustal growth: U–Pb and Sr–Nd isotopic evidence from the granites in northeastern China. Tectonophysics 328 (1–2), 89–113.
Wu, F.-Y., Sun, D.-Y., Li, H.-M., Wang, X.-L., 2001. The nature of basement beneath the Songliao basin in NE China: geochemical and isotopic constraints. Physics and Chemistry of the Earth, Part A: Solid Earth and Geodesy 26 (9–10), 793–803.
Wu, F.-Y., Sun, D.-Y., Li, H.-M., Jahn, B.-M., Wilde, S., 2002. A-type granites in northeastern China: age and geochemical constraints on their petrogenesis. Chemical Geology 187 (1–2), 143–173.
Wu, F.-Y., Jahn, B.-M., Wilde, S.A., Lo, C.-H., Yui, T.-F., Lin, Q., Ge, W.-C., Sun, D.-Y., 2003a. Highly fractionated I-type granites in NE China (I): geochronology and petrogenesis. Lithos 66 (3–4), 241–273.
Wu, F.-Y., Jahn, B.-M., Wilde, S.A., Lo, C.-H., Yui, T.-F., Lin, Q., Ge, W.-C., Sun, D.-Y., 2003b. Highly fractionated I-type granites in NE China (II): isotopic geochemistry and implications for crustal growth in the Phanerozoic. Lithos 67 (3–4), 191–204.
Wu, F.-Y., Yang, J.-H., Wilde, S.A., Liu, X.-M., Guo, J.-H., Zhai, M.-G., 2007. Lu–Hf isotope systematics and their applications in petrology. Acta Petrologica Sinica 23 (2), 185–220 (in Chinese with English abstract).
Wu, F.-Y., Xu, Y.-G., Gao, S., Zhang, H.-F., Zheng, J.-P., 2008. Lithospheric thinning and destruction of the North China Craton. Acta Petrologica Sinica 24, 1145–1174 (in Chinese with English abstract).
Xiao, W.-J., Windley, B.-F., Hao, J., Zhai, M.-G., 2003. Accretion leading to collision and the Permian Solonker suture, Inner Mongolia, China: termination of the central Asian orogenic belt. Tectonics 22 (6), 1069.
Xu, Y.G., 2001. Thermo-tectonic destruction of the Archean lithospheric keel beneath eastern China: evidence, timing and mechanism. Physics and Chemistry of the Earth, Part A: Solid Earth and Geodesy 26, 747–757.
Xu, Y.G., 2007. Diachronous lithospheric thinning of the North China Craton and formation of the Daxin'anling–Taihangshan gravity lineament. Lithos 96, 281–298.
Xu, Y.-G., Ma, J.-L., Huang, X.-L., Iizuka, Y., Chung, S.-L., Wang, Y.-B., Wu, X-Y., 2004a. Early Cretaceous gabbroic complex from Yinan, Shandong Province: petrogenesis and mantle domains beneath the North China Craton. International Journal of Earth Sciences 93, 1025–1041.
Xu, Y.-G., Huang, X.-L., Ma, J.-L., Wang, Y.-B., Iizuka, Y., Xu, J.-F., Wang, Q., Wu, X.-Y., 2004b. Crust–mantle interaction during the tectono-thermal reactivation of the North China Craton: constraints from SHRIMP zircon U–Pb chronology and geochemistry of Mesozoic plutons from western Shandong. Contributions to Mineralogy and Petrology 147, 750–767.
Xu, Y.-G., Li, H.-Y., Pang, C.-J., He, B., 2009. On the time and duration of the destruction of the North China Craton. Chinese Science Bulletin 54, 3379–3396.
Yang, W., Li, S.-G., 2008. Geochronology and geochemistry of the Mezozoic volcanic rocks in western Liaoning: implications for lithospheric thinning of the North China Craton. Lithos 102, 88–117.
Yang, J.-H., Wu, F.-Y., Shao, J.-A., Wilde, S.A., Xie, L.-W., Liu, X.-M., 2006. Constraints on the timing of uplift of the Yanshan Fold and Thrust Belt, North China. Earth and Planetary Science Letters 246 (3–4), 336–352.
Yuan, H.-L., Gao, S., Liu, X.-M., Li, H.-M., Günther, D., Wu, F.-Y., 2004. Accurate U–Pb age and trace element determinations of zircon by laser ablation-Inductively Coupled Plasma Mass Spectrometry. Geostandards and Geoanalytical Research 28, 353–370.
Zhang, Y.-Q., Dong, S.-W., Shi, W., 2003. Cretaceous deformation history of the middle Tan-Lu fault zone in Shandong Province, eastern China. Tectonophysics 363 (3–4), 243–258.
Zhang, S.-H., Zhao, Y., Song, B., 2006. Hornblende therobarometry of the carboniferous granitoids from the Inner Mongolia Paleo-uplift: implication for the geotectonic evolution of the northern margin of North China block. Mineralogy and Petrology 87 (1–2), 123–141.
Zhang, S.-H., Zhao, Y., Song, B., Yang, Z.-Y., Hu, J.-M., Wu, H., 2007a. Carboniferous granitic plutons from the northern margin of the North China block: implications for a late Palaeozoic active continental margin. Journal of the Geological Society 164 (2), 451–463.
Zhang, S.-H., Zhao, Y., Song, B., Yang, Y.-H., 2007b. Zircon SHRIMP U–Pb and in situ Lu–Hf isotope analyses of a tuff from Western Beijing: evidence for missing Late Paleozoic arc volcano eruptions at the northern margin of the North China block. Gondwana Research 12 (1–2), 157–165.
Zhang, S.-H., Zhao, Y., Song, B., Liu, D.-Y., 2007c. Petrogenesis of the Middle Devonian Gushan diorite pluton on the northern margin of the North China block and its tectonic implications. Geological Magazine 144 (3), 553–568.
Zhang, S.-H., Zhao, Y., Liu, X.-C., Liu, D.-Y., Chen, F.-K., Xie, L.-W., Chen, H.-H., 2009. Late Paleozoic to Early Mesozoic mafic-ultramafic complexes from the northern North China block: constraints on the composition and evolution of the lithospheric mantle. Lithos 110, 229–246.
Zhang, S.-H., Zhao, Y., Song, B., Hu, J.-M., Liu, S.-W., Yang, Y.-H., Chen, F.-K., Liu, X.-M., Liu, J., 2009a. Contrasting Late Carboniferous and Late Permian–Middle

Triassic intrusive suites from the northern margin of the North China craton: geochronology, petrogenesis, and tectonic implications. Geological Society of American Bulletin 121 (1–2), 181–200.

Zhang, S.-H., Zhao, Y., Kröner, A., Liu, X.-M., Xie, L.-W., Chen, F.-K., 2009b. Early Permian plutons from the northern North China block: constraints on continental arc evolution and convergent margin magmatism related to the Central Asian orogenic belt. International Journal of Earth Sciences 98 (6), 1441–1467.

Zhao, G.C-., Wilde, S.A., Cawood, P.A., Sun, M., 2001. Archean blocks and their boundaries in the North China Craton: lithological, geochemical, structural and P-T path constraints. Precambrian Research 107, 45–73.

Zhao, G.-C., Wilde, S.A., Li, S.-Z., Sun, M., Grant, M.-L., Li, X.-P., 2007. U-Pb zircon age constraints on the Dongwanzi ultramafic-mafic body, North China, confirm it is not an Archean ophiolite. Earth and Planetary Science Letters 255 (1–2), 85–93.

Zhou, M.-F., Zhao, J.-H., Xia, X.-P., Sun, W.-H., Yan, -D.-P., 2007. Comment on "Revisiting the "Yanbian Terrane": implications for Neoproterozoic tectonic evolution of the western Yangtze block, South China" [Precambrian Res. 151 (2006) 14–30]. Precambrian Research 155 (3–4), 313–317.

Zhu, R.-X., Yang, Z.-Y., Wu, H.-N., Ma, X.-H., Huang, B.-C., Meng, Z.-F., Fang, D.-J., 1998. Paleomagnetic constraints on the tectonic history of the major blocks of China during the Phanerozoic. Science in China Series D Earth Science 41 (S2), 1–19.